

Maintaining stimulant waveforms in large-volume microfluidic cell chambers

Xinyu Zhang · Raghuram Dhumpa ·
Michael G. Roper

Received: 28 August 2012 / Accepted: 13 December 2012 / Published online: 28 December 2012
© Springer-Verlag Berlin Heidelberg 2012

Abstract Stimulation of cells with temporal waveforms can be used to observe the frequency-dependent nature of cellular responses. The ability to produce and maintain the temporal waveforms in spite of the broadening processes that occur as the wave travels through the microfluidic system is critical for observing dynamic behaviors. Broadening of waves in microfluidic channels has been examined, but the effect that large-volume cell chambers have on the waves has not. In this report, a sinusoidal glucose wave delivered to a 1-mm diameter cell chamber using various microfluidic channel structures was simulated by finite element analysis with the goal of minimizing the broadening of the waveform in the chamber and maximizing the homogeneity of the concentration in the chamber at any given time. Simulation results indicated that increasing the flow rate was the most effective means to achieve these goals, but at a given volumetric flow rate, geometries that deliver the waveform to multiple regions in the chamber while maintaining a high linear velocity produced sufficient results. A 4-inlet geometry with a 220- μm channel width gave the best result in the simulation and was used to deliver glucose waveforms to a population of pancreatic islets of Langerhans. The result was a stronger and more robust synchronization of the islet population as compared with when a non-optimized chamber was used. This general strategy will be useful in other microfluidic systems examining the frequency-dependence nature of cellular behavior.

Keywords Dynamic stimulation · Microfluidic perfusion · Finite element analysis · Broadening and delay · Islets of Langerhans

1 Introduction

Microfluidic systems are increasingly used to evaluate the dynamic nature of biological systems, for example, genetic networks (Lucchetta et al. 2005; Danino et al. 2010), transcriptional responses (King et al. 2008), or protein expression (Mondragon-Palomino et al. 2011). In these investigations, temporally varying concentrations of stimulant are used to probe the frequency-dependence of cellular responses, which can reveal features of cellular responses not observed by stimulation with a single concentration of stimulant (Jovic et al. 2010; Dhumpa and Roper 2012). One challenge in using temporal gradients is dispersion of the waveform as they pass through the fluidic system.

All dispersive channels are low-pass filters since high-frequency chemical waves will disperse at a greater rate than low-frequency waves (Azizi and Mastrangelo 2008). The result of this low-pass filtering is broadening and amplitude attenuation of the output waveforms. The amount of attenuation, described as the ratio of the output to input concentrations, is a function of channel length (L) and input frequency (f) (Azizi and Mastrangelo 2008):

$$\left\| \frac{C_{\text{out}}(f, L)}{C_{\text{in}}(f, 0)} \right\| \approx \exp\left(-\frac{f^2}{f_c^2}\right) \quad (1)$$

where C_{out} is the concentration of the output waveform amplitude, C_{in} is the concentration of the input waveform amplitude, and f_c is the cutoff frequency. f_c is approximated as

X. Zhang · R. Dhumpa · M. G. Roper (✉)
Department of Chemistry and Biochemistry,
Florida State University, 95 Chieftan Way,
Dittmer Building, Tallahassee, FL 32306, USA
e-mail: roper@chem.fsu.edu

$$f_c \approx \left[\frac{V^3}{DL} \right]^{1/2} \quad (2)$$

where V is the linear flow velocity and D is the effective Taylor dispersion-adjusted diffusion coefficient (Xie et al. 2008). Based on Eqs. 1 and 2, to ensure cells receive the true waveform, a large f_c of the device is required, which dictates high velocities and/or short channel lengths.

Most reports using temporal gradients have utilized microfluidic devices that hold cells within the channels allowing Eqs. 1 and 2 to accurately reflect the attenuation of the waveform in the cell chamber. However, when large-volume cell chambers or irregular cell chamber geometries are used, it is more difficult to predict the attenuation. The homogeneity of the stimulant waveform across the cell chamber is not taken into account using Eqs. 1 or 2, but is an important feature to consider so that all cells experience the same concentration of stimulant at any given time. It would be ideal if both of these features, attenuation of the waveforms and homogeneity across the cell chamber, could be predicted to aid in the design of large-volume cell chambers used for dynamic stimulation.

In this work, the geometrical factors of the microfluidic system that are important for maintaining waveforms in large-volume cell chambers are reported. The testing and optimization of microfluidic geometries were performed using finite element analysis (FEA) to model sinusoidal waves that entered a 1-mm diameter chamber. Multiple microfluidic geometries were tested to find the optimum conditions that resulted in the lowest attenuation and highest uniformity of the stimulus waveform in the cell chamber at any time. To demonstrate the significance of this work, the results from stimulating ~ 20 islets of Langerhans with glucose waveforms in optimized and non-optimized chambers are compared.

2 Experimental

2.1 Simulation

COMSOL Multiphysics (Los Angeles, CA) was used to build the finite element models. 3D cell chambers were drawn and meshed using tetrahedral finite elements. In all simulations, Navier–Stokes equations were first solved for a stationary velocity profile of creeping flows. In all model geometries, different linear velocities were used as initial conditions such that the total volumetric flow rate into each chamber was 0.5, 1.0, or 1.5 $\mu\text{L}/\text{min}$. The walls in the model were no slip, the outlet was set with no viscous stress, and all liquids were defined with a density of 1,000 kg/m^3 and a viscosity of 0.001 Pa s. After the velocity profile was solved, parabolic partial differential

equations for convection and diffusion were solved for time-dependent profiles of the concentration gradients using a diffusion coefficient of $10^{-5} \text{ cm}^2/\text{s}$. All input waveforms were sinusoidal with a period of 5 min, a median concentration of 11 mM, and amplitude of 1 mM. In initial simulations, 20 spheres each of 130 μm diameter, located on the chamber floor, were included in the simulation to mimic the effect of islets on the flow streamlines. After each simulation was completed, a 2D slice of the concentration profile at the floor of the chamber ($z = 0$) was exported and analyzed using ImageJ software (National Institutes of Health, USA; <http://rsb.info.nih.gov>) for calculations. The concentration values within the inlets were not included in any calculations.

2.2 Chemicals and reagents

HNO_3 , CaCl_2 , NaOH , and NaCl were purchased from EMD Chemicals, Inc. (Gibbstown, NJ). Polydimethylsiloxane (PDMS) was from Rogers Corporation (Carol Stream, IL). Glucose (dextrose), MgCl_2 , HF and Cosmic Calf Serum were from Fisher Scientific (Pittsburgh, PA). KCl, fluorescein, tricine, dimethyl sulfoxide (DMSO) and Type XI collagenase were from Sigma (St. Louis, MO). Fura-2 acetoxymethyl ester (fura-2 AM), Pluronic F-127, RPMI 1640 with 11 mM glucose, and penicillin–streptomycin were from Invitrogen (Carlsbad, CA). All solutions were made with Milli-Q (Millipore, Bedford, MA) 18 M Ω cm deionized water. The buffer solution used in all experiments contained 2.4 mM CaCl_2 , 125 mM NaCl , 1.2 mM MgCl_2 , 5.9 mM KCl and 25 mM tricine, and this buffer was used to make 100 μM fluorescein as well as 3 and 13 mM glucose.

2.3 Chip design and pumping program

The device was fabricated via photolithography and chemical etching as described previously (Zhang et al. 2011). The microfluidic chip had two on-chip diaphragm pumps that delivered 13 and 3 mM glucose solutions through a mixing channel of $220 \times 90 \mu\text{m} \times 3.3 \text{ cm}$ (width \times depth \times length) into a cell chamber. The diaphragm pumps were controlled by a program written in LabView (National Instruments, Austin, TX) via a data acquisition card (NI PCI-6221) and solenoid valves (model A00SC232P, Parker Hannifin Corp., Cleveland, OH). For all experiments, the volumetric flow rate into the chamber was 1.5 $\mu\text{L}/\text{min}$.

The cell chamber was drilled using diamond-tipped drill bits (Norton Abrasives, North Tonawanda, NY) and all chambers had a height of 1.0 mm due to the thickness of the glass. In all experiments, a controller (CNi 3233, Omega Engineering, Inc., Stamford, Connecticut), a thermofoil (KHLV-0502/5, Omega Engineering), and a thermocouple

sensor (SA1-J, Omega Engineering) were attached to the microfluidic chip to maintain the temperature of the cell chamber at 37 °C.

2.4 Dynamic stimulation of islets of Langerhans

Islets of Langerhans were collected as previously described (Zhang et al. 2011). To examine the effects of dynamic stimulation on islets of Langerhans, intracellular $[Ca^{2+}]_i$ ($[Ca^{2+}]_i$) was monitored by fura-2 fluorescence. To load fura-2 into islets, 1.0 μ L of 5.0 mM fura-2 AM in DMSO and 1.0 μ L Pluronic F-127 in DMSO were mixed and transferred into 2 mL RPMI to form a final fura-2 AM concentration of 2.5 μ M. Islets were incubated in this solution at 37 °C and 5 % CO_2 for 45 min and then were transferred to the islet chamber in the microfluidic device, where islets were perfused with 3 mM glucose prior to recording fura-2 fluorescence.

2.5 Measurement of fura-2 fluorescence

The microfluidic device was placed on the stage of a Nikon Eclipse Ti microscope for all experiments. A broadband lamp (Lambda XL, Sutter Instrument, Novato, CA) integrated with a filter wheel containing two filters (XF1093 and XF1094, Omega Optical, Brattleboro, VT) at 340 nm and 380 nm was used to excite fura-2. A shutter was used to minimize photobleaching of the fura-2 by opening 150 ms for each filter, every 10 s. The excitation light was filtered by neutral density filters (XB17, Omega Optical), reflected by a dichroic mirror (XF2002), and focused onto the islet chamber through a 10 \times , 0.5 NA or 40 \times , 0.6 NA UV-compatible objective. The fura-2 emission, collected by the same objective, passed through the dichroic mirror and an emission filter (XF3043) and made incident on a CCD camera (Cascade, Photometrics, Tucson, AZ) for imaging. NIS-Elements (Nikon, Melville, NY) was used to control the Sutter filter wheel, shutter, and CCD camera. All measurements of fura-2 fluorescence are reported as the ratio of fura-2 emission at 520 nm upon excitation by 340 nm and 380 nm (F_{340}/F_{380}). The F_{340}/F_{380} ratio is proportional to $[Ca^{2+}]_i$ (Grynkiewicz et al. 1985).

3 Results and discussion

Large-volume cell chambers are used in microfluidics research to hold large numbers of cells (Clark et al. 2010) or large diameter cells (Mohammed et al. 2009; Sankar et al. 2011). While most applications with these chambers have involved step changes of stimulant concentrations, stimulation with dynamic changes can reveal cellular behavior that is not typically observed under static conditions.

As an example, we have utilized microfluidic systems to produce and deliver sinusoidally varying glucose concentrations to islets of Langerhans to investigate the dynamics of these micro-organs (Zhang et al. 2010; Zhang et al. 2011). Glucose oscillations have been observed in vivo and it has been hypothesized that these oscillations synchronize islets of Langerhans in the pancreas (Sturis et al. 1994; Chou and Ipp 1990). We (Zhang et al. 2010), and others (Chou and Ipp 1990; Sturis et al. 1994) have shown that single islets can be forced, or entrained, by glucose waves. Recently, we demonstrated that ~ 20 islets can be entrained to a glucose waveform producing a synchronized response from the islet population (Zhang et al. 2011). However, because each islet was ~ 150 μ m diameter, the use of the large number of islets necessitated the use of a larger chamber (1 mm diameter) than what we used for single islet entrainment (0.5 mm diameter). When initial experiments failed to entrain 20 islets using the large chamber, we found that increasing the number of waveform inputs into the chamber allowed the islets to be entrained. We hypothesized that this design minimized waveform attenuation and produced a homogeneous glucose concentration across the large chamber allowing all 20 islets to experience the same wave and become entrained. In this report, we set out to quantitatively examine the geometrical features of the microfluidic system that will increase waveform homogeneity over large-volume cell chambers to make these approaches applicable to other cell types or other microfluidic systems.

3.1 Broadening and delay of waves

Our initial goal was to understand why islets could be entrained when a 0.5-mm diameter chamber was used, but not the initial attempts when a 1-mm diameter chamber was used. FEA was utilized for investigating the waveform behavior because the chamber geometry was more complex than the geometries that were assumed in developing Eqs. 1 and 2.

Figure 1a shows a 3D view of a simulated 1 mm chamber located at the end of a perfusion channel. The volumetric flow rate into the chamber was 1.5 μ L/min, and the glucose concentration is shown by the colors, with red being a higher concentration and blue being a lower concentration. Figure 1b shows a 2D slice through the chamber. In Fig. 1a and b, the fluid streamlines are shown in red and indicated that the majority of the perfusate exits the chamber instead of reaching the far end of the chamber to replace the liquid. The result is considerable heterogeneity of the glucose concentration across the chamber floor where the islets would be located. For example, two islets, one placed at the chamber entrance and the other on the other side of the chamber, would sense different glucose

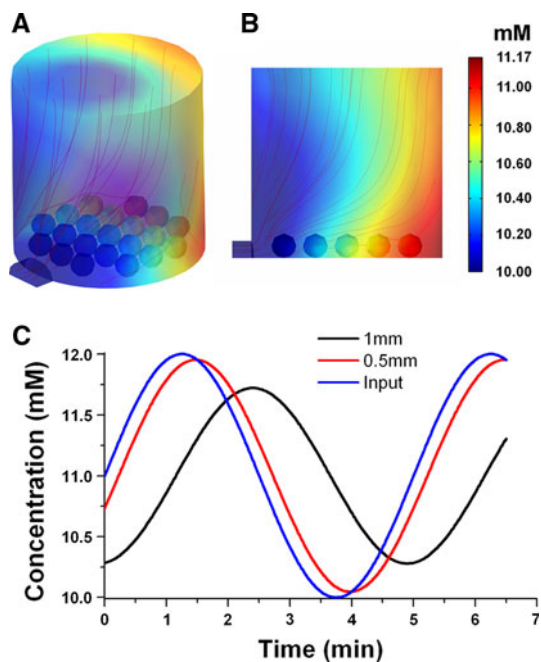


Fig. 1 Broadening of glucose waves and concentration heterogeneity in a large microfluidic chamber. **a** The 3-dimensional model of a 1×1 mm (diameter \times height, $0.8 \mu\text{L}$) cylindrical chamber is shown. A section of the fluid channel and 20 islets were included in the simulation. The *red lines* are fluid streamlines and the *colors* show the glucose concentration according to the *scale bar* on the *right*. **b** A 2D slice through the center of the chamber shown in **a**. **c** The input glucose waveform is shown in *blue* and the wave measured across a 1-mm chamber is shown in *black*. The *red curve* is the resulting concentration profile when the same input wave was delivered to a 0.5-mm chamber

concentrations at a given time and would not synchronize. In order for all the islets in the chamber to synchronize, they all need to experience the same glucose concentration, which would only occur when a homogeneous glucose concentration across the chamber floor is produced. This result would be shown as a single color along the bottom of the 2D slice shown in Fig. 1b.

While Fig. 1a and b is indicative of the glucose concentration at an instant in time, Fig. 1c shows the concentration profile of the stimulus waveform at different locations in the cell chamber over a longer time. The blue curve (input) is the concentration of the waveform as it enters the cell chamber and the black curve is the concentration on the chamber floor at the opposite side of a 1-mm diameter chamber. Compared with the input wave, there was significant amplitude attenuation as the wave traveled across the chamber, and the phase offset between the two waves indicates the difference in glucose concentration that two islets would feel at these locations in the chamber at an instant in time. When a 0.5 mm diameter chamber was simulated (red curve), both the attenuation and phase offset were reduced, indicating a more homogeneous glucose concentration across the chamber. This

better result with the smaller chamber was due to a higher linear velocity than what occurs in a 1-mm diameter chamber, so that smaller chamber volume can be replaced quickly ensuring all islets in the chamber feel approximately the same glucose concentration.

To quantify both the broadening of waves and concentration heterogeneity at the chamber bottom, the amplitude attenuation and standard deviation of the concentration in the chamber were evaluated by a “*W*-index”:

$$W = \frac{\text{Amplitude response}}{\text{SD of concentrations}} \quad (3)$$

In this equation, amplitude response was defined similarly as before (Zhang et al. 2010) as the ratio of the lowest to highest amplitudes in the chamber at any instant in time. The highest amplitude was found at the input of the chamber, whereas the lowest amplitude was on the opposite end of the chamber. In other microfluidic designs discussed later, the lowest amplitude position may be in a different location. Ideally, the amplitude at the two locations would be equal resulting in an amplitude response of 1. The denominator reflected the concentration distribution over the entire chamber bottom when the input concentration reached the maximum. In the best-case scenario, the distribution would be close to zero. Therefore, a chamber geometry that maintained the waveform throughout the chamber would have a high *W*-index. The *W*-index calculated for a 0.5 and 1 mm chamber was 86.5 and 2.38, respectively. We found little difference when islets were added to the model, and they were therefore removed from later simulations.

3.2 Geometrical modification

In an attempt to make the concentration in the cell chamber more homogeneous, several geometrical parameters of the device were modified while maintaining the cell chamber at 1 mm diameter. Both the width and number of channels delivering waves to the islet chamber were increased in an attempt to deliver the glucose wave to a larger area of the cell chamber. A series of models were then constructed containing 1, 2, 4, and 8 inlets. Each of these models was further varied by changing the width of the inlet channel by an integer multiple of the initial channel width of $220 \mu\text{m}$, called 1X, 2X, and 4X. All chamber designs were modeled using a total flow rate of 0.5, 1.0, and $1.5 \mu\text{L}/\text{min}$ into the chamber to investigate the influence of velocity on the *W*-index. Figure 2 details the results of the models at a flow rate of $0.5 \mu\text{L}/\text{min}$. Each row in Fig. 2 shows a different number of input channels, and each column shows a different width of the input channels. In some of the designs with multiple input channels, not all widths could be tested because the sum of all channel widths would be larger than the chamber perimeter.

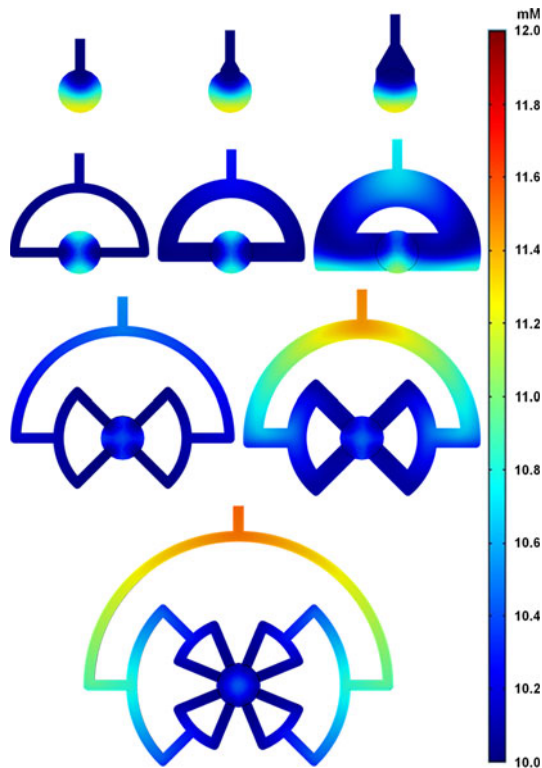


Fig. 2 Cell chambers with different numbers of inlets and channel widths. The *top row* shows the 1-inlet results, the *2nd row* is the 2-inlet results, the *3rd row* is the 4-inlet results, and the *4th row* is the 8-inlet results. On the *top 3 rows*, the far *left* image is the 1X channel width corresponding to 220 μm , the next image is the 2X channel width, and the *1st* and *2nd row* show a 4X channel width on the *right*. The 8-inlet system could only simulate a 1X channel width. The dead volume mentioned in the text can be seen in the 2-inlet, 4X design at the *bottom* of the turns. In all images shown, the glucose waves were delivered at a total flow rate of 0.5 $\mu\text{L}/\text{min}$ and the input concentrations at the chamber entrance were 10 mM to make the concentration distribution in the chambers easier to visualize

As expected, with the 1-inlet design, homogeneity across the chamber was low and the W -index at all flow rates and channel widths was below 5 (Fig. 3). High flow rates increased the W -index, which applied to all designs and was in agreement with Eq. 2. For the 1-inlet design, the W -index was highest when a channel width of 4X was used even though this configuration produced the lowest linear flow velocity as compared with 1X and 2X at a given volumetric flow rate. This result reflected that in a complex geometry like the cell chamber, it is difficult to infer how the velocity and geometry influence the W -index.

With the 2-inlet design, the standard deviation of the concentration distribution across the cell chamber decreased compared with the 1-inlet design, which resulted in an increased W -index, although it never rose above 10 for any 2-inlet design tested. Furthermore, the W -index of the 4X design was clearly lower than the 2X design, which indicated that the reduction in linear velocity due to the

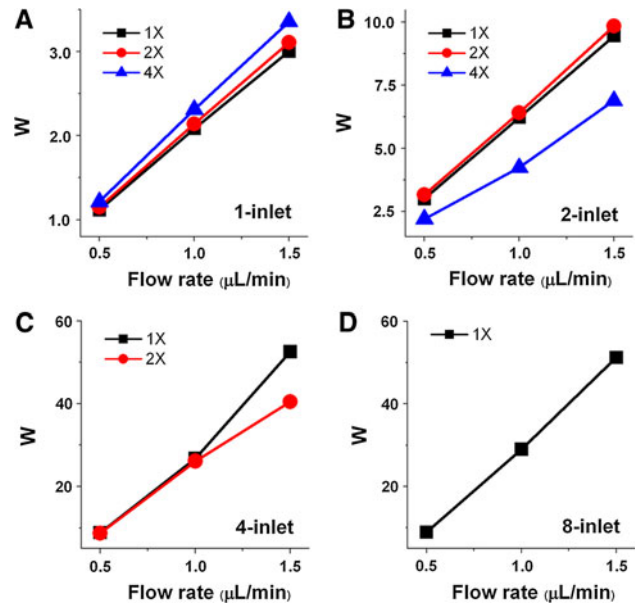


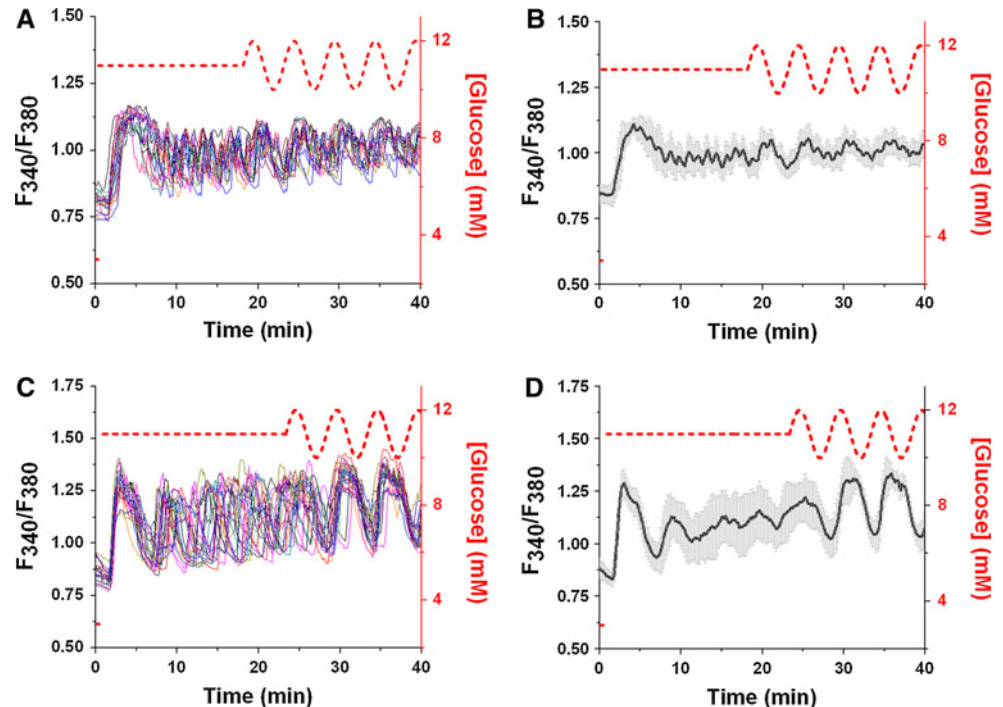
Fig. 3 W -indices in cell chambers with different designs. W -indices as a function of the numbers of inlets (**a** = 1-inlet, **b** = 2-inlet, **c** = 4-inlet, and **d** = 8-inlet), channel widths (*black* = 1X, *red* = 2X, and *blue* = 4X), and flow rates are shown

broader channels could not compensate for the increased area from the 2 inlets. Figure 2 also shows that with the 4X design, the concentration heterogeneity in the chamber was in part attributed to the channel network that was used leading to the chamber. A lower velocity was present at the corners of the turns prior to the cell chamber, which resulted in broadening of the waveforms. This effect was not noticed at the smaller channel widths because the linear velocity was higher and able to minimize dead volume.

It was not until the 4-inlet design that the W -index increased above a value of 30, which we deemed as suitable for producing homogeneous concentrations in the chamber. Similar to the 2-inlet design, a lower W -index was observed with the 2X design compared with the 1X, due to the lowered linear velocity and the presence of the dead volume at the turns. In the 8-inlet design, only the 1X channel width could be tested. While the waveforms were delivered to a larger proportion of the cell chamber compared with the 4-inlet design, the linear velocity was lower and the increased number of turns in the channel network resulted in increased dead volume. The final W -indices at 1.5 $\mu\text{L}/\text{min}$ for the 4-inlet 1X design and the 8-inlet design were 53 and 51, respectively.

To summarize, the most effective way to increase the W -index was to increase the flow rate, but at a given flow rate, increasing the number of inlets was another suitable method. However, due to both the presence of dead volume and the subsequent decrease in linear flow rate with increased channel branching, there appears to be an optimum number of inlets.

Fig. 4 Fura-2 fluorescence from islets within a 1- and 4-inlet, 1X design. In all graphs, $[Ca^{2+}]_i$ was measured by fura-2 fluorescence as described in the “Experimental” section and is plotted on the left y-axes. The glucose profile is shown as a dashed red line and corresponds to the right y-axes. In all results, a 1-mm diameter islet chamber was used. **a** Fura-2 traces from 18 islets when a 1-inlet, 1X design was used. The glucose concentration was oscillated at ~ 18 min. **b** The average F_{340}/F_{380} trace from all islets in **a** is shown with error bars corresponding to ± 1 SD. **c** Fura-2 traces from 21 islets when a 4-inlet, 1X design was used. The glucose concentration was oscillated at ~ 23 min. **d** The average F_{340}/F_{380} ratio of the traces shown in **c** with error bars corresponding to ± 1 SD



3.3 Comparison of optimized versus non-optimized geometries for islet synchronization

To compare how the microfluidic geometry could affect the biological results, a 1- and 4-inlet, 1X designs with a 1-mm diameter chamber were fabricated. Approximately 20 islets were loaded with the $[Ca^{2+}]_i$ -indicator, fura-2, and placed in each chamber and the fura-2 fluorescence was monitored. Figure 4a and b shows the individual and average fura-2 signals from islets in the 1-inlet chamber and Fig. 4c and d are the individual and average fura-2 signals from islets in the 4-inlet chamber. In all experiments, the glucose concentration began at 3 mM and was then raised to 11 mM for observing free-running $[Ca^{2+}]_i$ oscillations. During this free-running period, each islet oscillated independently as shown in Fig. 4a and c. This is expected under free-running conditions and is clearly observed by the lack of synchronization in the average fura-2 traces (Fig. 4b and d).

After a short time, the glucose concentration was oscillated in a sinusoidal manner with 1 mM amplitude and 300 s period. Although it is difficult to observe in Fig. 4a, the islets did entrain to a small extent in the 1-inlet design. This synchronization is more readily observable in Fig. 4b where the average fura-2 trace shows slight oscillations after the periodic glucose signal was applied. However, the islets in the 4-inlet device clearly became entrained within a single period of the glucose wave (Fig. 4c). The average fura-2 signal from all 20 islets shows strong and coherent oscillations from the islet population (Fig. 4d). The fura-2

oscillations were not as robust or as strongly synchronized in the 1-inlet device compared with the 4-inlet device.

These results confirmed that a large W -index would produce a more synchronized population, whereas a low W -index could hamper the observation of this behavior. Although we did not experimentally determine the cutoff between a low and high W -index, a value of 30 was found to be a good estimate as to the ability to synchronize the population or not.

4 Conclusion

Finite element analysis was used to investigate the influence of the microfluidic geometry on the broadening of stimulus waveforms and concentration heterogeneity in large cell chambers. The simulations showed the 4-inlet 1X design to be optimal and were confirmed by measuring synchronization of islet oscillations, which are sensitive to the stimulus waveforms in the chamber. In the simulations presented here, and as evidenced by the synchronized fura-2 oscillations, the presence of the islets in the chamber did not hamper the waveforms, but in other situations, they may induce unforeseen flow patterns which may need to be taken into account. Also, a W -index of 30 as the cutoff between a functional and non-functional chamber was chosen arbitrarily and for other applications may be different. Other facets of the microfluidic geometry could also be investigated to produce a more homogeneous waveform in the chamber, for example, the geometry of the cell

chamber itself. Finally, this method of maintaining temporal waveforms in large chambers may be suitable for investigations of cellular dynamics in other systems where large cell numbers or tissue slices are required.

Acknowledgments This work was supported in part by a grant from the National Institutes of Health (R01 DK080714). The authors thank Tuan Truong for help with isolating islets of Langerhans.

References

- Azizi F, Mastrangelo CH (2008) Generation of dynamic chemical signals with pulse code modulators. *Lab Chip* 8:907–912
- Chou HF, Ipp E (1990) Pulsatile insulin secretion in isolated rat islets. *Diabetes* 39:112–117
- Clark AM, Sousa KM, Chisolm CN, MacDougald OA, Kennedy RT (2010) Reversibly sealed multilayer microfluidic device for integrated cell perfusion and on-line chemical analysis of cultured adipocyte secretions. *Anal Bio Chem* 397:2939–2947
- Danino T, Mondragon-Palomino O, Tsimring L, Hasty J (2010) A synchronized quorum of genetic clocks. *Nature* 463:326–330
- Dhumpa R, Roper MG (2012) Temporal gradients in microfluidic systems to probe cellular dynamics: a review. *Anal Chim Acta* 743:9–18
- Gryniewicz G, Poenie M, Tsien RY (1985) A new generation of Ca^{2+} indicators with greatly improved fluorescence properties. *J Biol Chem* 260:3440–3450
- Jovic A, Howell B, Cote M, Wade SM, Mehta K, Miyawaki A, Neubig RR, Linderman JJ, Takayama S (2010) Phase-locked signals elucidate circuit architecture of an oscillatory pathway. *PLoS Comput Biol* 6:e1001040
- King KR, Wang S, Jayaraman A, Yarmush ML, Toner M (2008) Microfluidic flow-encoded switching for parallel control of dynamic cellular microenvironments. *Lab Chip* 8:107–116
- Lucchetta EM, Lee JH, Fu LA, Patel NH, Ismagilov RF (2005) Dynamics of *Drosophila* embryonic patterning network perturbed in space and time using microfluidics. *Nature* 434:1134–1138
- Mohammed JS, Wang Y, Harvat TA, Oberholzer J, Eddington DT (2009) Microfluidic device for multimodal characterization of pancreatic islets. *Lab Chip* 9:97–106
- Mondragon-Palomino O, Danino T, Selimkhanov J, Tsimring L, Hasty J (2011) Entrainment of a population of synthetic genetic oscillators. *Science* 333:1315–1319
- Sankar KS, Green BJ, Crocker AR, Verity JE, Altamentova SM et al (2011) Culturing pancreatic islets in microfluidic flow enhances morphology of the associated endothelial cells. *PLoS ONE* 6:e24904
- Sturis J, Pugh WL, Tang JP, Ostrega DM, Polonsky JS, Polonsky KS (1994) Alterations in pulsatile insulin secretion in the Zucker diabetic fatty rat. *Am J Physiol* 267:E250–E259
- Xie Y, Wang Y, Chen L, Mastrangelo CH (2008) Fourier microfluidics. *Lab Chip* 8:779–785
- Zhang XY, Grimley A, Bertram R, Roper MG (2010) Microfluidic system for generation of sinusoidal glucose waveforms for entrainment of islets of Langerhans. *Anal Chem* 82:6704–6711
- Zhang XY, Daou A, Truong T, Bertram R, Roper MG (2011) Synchronization of mouse islets of Langerhans by glucose waveforms. *Am J Physiol Endocrinol Metab* 301:E742–E747